

Supernova Science with an Advanced Compton Telescope

P.A. Milne ¹, R.A. Kroeger ², L.-S. The ³

1 NRC/NRL Resident Research Associate, Naval Research Lab, Code 7650, Washington DC 20375

2 Naval Research Lab, Code 7650, Washington DC 20375

3 Clemson University, Clemson, SC 29634

ABSTRACT Gamma-ray line emission is a direct probe of the nucleosynthesis that occurs in Type Ia supernovae. In this work we describe the wealth of information obtainable from observations of this emission. Advanced Compton telescope designs are being studied by the Naval Research Laboratory, with the goal being the construction of a telescope which would be capable of detecting SNe Ia to distances in excess of 100 Mpc. We describe the instrument capabilities and the design issues that are being addressed. We assume a SN Ia rate and quantify the frequency at which an advanced Compton telescope could detect, discriminate between, and diagnose Type Ia supernovae. From these estimates, we argue that an advanced Compton telescope would be a powerful astrophysical tool.

KEYWORDS: gamma rays:observations - Galaxy: center - supernovae: general - ISM: general

1. INTRODUCTION

A supernova (SN) is the brilliant death of a star. Due to the thermonuclear explosion of a CO white dwarf (SN Ia) or to the core-collapse of a massive star (SN II/Ib/Ic), supernovae (SNe) alter the composition of the progenitor object, impulsively synthesizing new isotopes. It was recognized in the 1960s that the decay of radionuclei was required to explain the light curves of supernovae (Colgate et al. 1966, Truran et al. 1967, Bodansky et al. 1968). The principal radionuclei studied have been ^{56}Ni and its daughter product ^{56}Co , but ^{57}Co , ^{44}Ti , ^{22}Na and ^{60}Co have also been suggested to contribute to the optical light (Woosley, Pinto & Hartmann 1989). The study of SN nucleosynthesis has branched into three principle categories; explosive nucleosynthesis, radiation transport, and galactic chemical evolution. The first category of study concentrates upon applying nuclear physics and magneto-hydrodynamics to simulate the evolution of the progenitor object(s) up to and through explosive nucleosynthesis. The results from these studies are; a) the determination of whether (or for what range of parameters) a given explosion scenario successfully yields a SN explosion, and b) the composition and kinematic structure of the ejecta of successful explosions, especially the yields of radionuclei. The second category of study accepts the outputs of the first group (SN models) and seeks to derive further constraints upon SNe through comparisons with observations. The key physics involved with these investigations are the transport of the decay products of the various radionuclei (γ /x-ray photons and positrons) and the subsequent diffusion and emission of UV/OPT/IR photons. The third category of study attempts to reproduce the local, galactic and extra-galactic abundances of all isotopes. The information critical to the third study is the exact nucleosynthesis contribution from SNe as a function of time and galaxy location.

The study of gamma-ray line emission is an excellent diagnostic of SNe which can contribute to

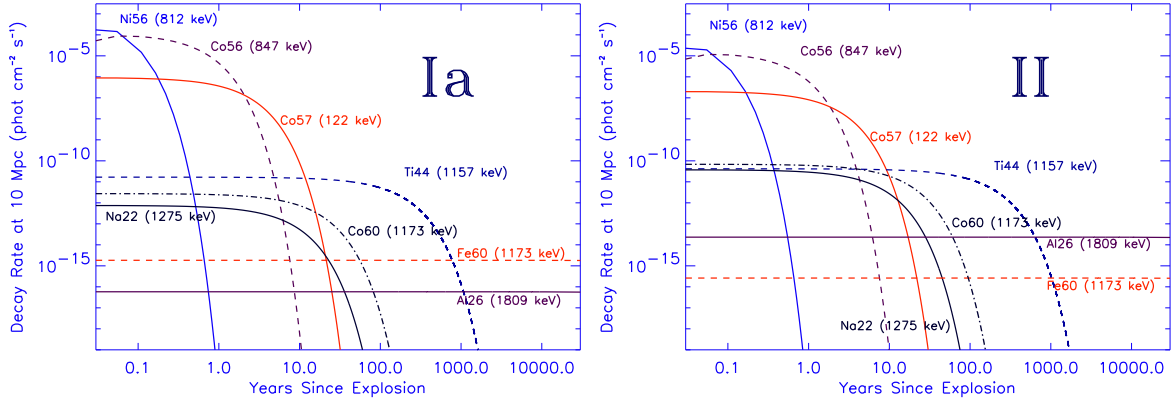


Figure 1. The decay rates of the SN Ia model, W7, and the SN II model, W10HMM.

Both SNe are at a distance of 10 Mpc. The large scale hides the difference of a factor of eight in the ^{56}Ni production between the two SN types.

all three investigations. In the following three sections, we discuss the science derived from gamma-ray line observations. In the first section, we discuss the physics of nuclear decays and the escape of gamma-ray photons. In the second section, we describe the specifications of an advanced Compton telescope (ACT), particularly the version being investigated at the Naval Research Lab (NRL). In the third section, we discuss the science that could be performed with an ACT. We conclude with an assessment of what we consider to be the priorities of SN science with an ACT.

1 Gamma-Ray Line Emission Physics

Radionuclei produced in SNe decay to stable nuclei on various time-scales, generating gamma- and x-ray photons, electrons and positrons. These decay products either deposit their energy in the ejecta (at early times helping to lift the ejecta, at later times driving the UV/OPT/IR light curves) or they escape, leading to potentially detectable γ /x-ray emission. Shown in Figure 1 are the decay curves for the principal radionuclides of two SN models.¹² The left panel shows the decay rates of the SN Ia model W7 (Nomoto et al. 1984). The right panel shows the decay rates for the SN II model W10HMM (Pinto & Woosley 1988). Evident in this figure is the cascade from the early-time dominance of short-lived radioactivities to the later dominance of long-lived radioactivities. Assuming that a large fraction of these photons escape, short-lived radioactivities give rise to intense, but brief emission, while long-lived radioactivities give rise to faint, but persistent emission. For the

¹This would be the flux observed if 100% the photons escape (*i.e.* zero opacity).

² The decay of $^{56}\text{Ni} \rightarrow ^{56}\text{Co}$ produces 750 & 1562 keV lines in addition to the 812 keV line. The decay of $^{56}\text{Co} \rightarrow ^{56}\text{Fe}$ produces a 1238 keV line in addition to the 847 keV line. The branching ratios are 0.49 (750), 0.86 (812), 0.14 (1562), 1.00 (847), 0.68 (1238) (Nadyozhin 1994).

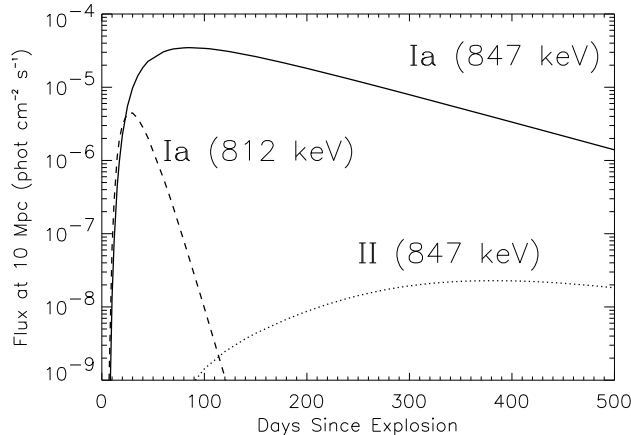


Figure 2. The 812 & 847 keV line fluxes for the same Type Ia and Type II models shown in Figure 1.

purposes of this work, the gamma emission is categorized as prompt, supernova remnant (SNR), or diffuse. This categorization is based upon both the physics of the gamma-ray emission (the opacity and the angular size of the emitting region) and upon the instruments employed to detect the emission.

Initially, the SN density is so large that all γ/x -ray photons are scattered and no high-energy emission emerges. As the SN expands, the ejecta thins and the γ/x -ray photons begin to escape. Thus, the *prompt* γ/x -ray line flux from a SN depends upon the overlying mass and the ejecta kinematics. This makes the evolution of the fluxes of the various gamma-ray lines a probe of the SN ejecta. The optical absorption and emission lines from SNe also probe these quantities, but not as early, nor as directly as do the gamma-ray lines. The *prompt* epoch is characterized by the lowering of the gamma-ray line opacity to negligible values. The early onset of gamma-ray escape would make prompt emission detectable to large distances. Although plausible SNe Ia and SNe II/Ib/Ic explosion scenarios exhibit a range of characteristics, the timescale of prompt emission is on the order of a year.

Two different approaches have been employed to detect SN gamma rays; wide-FoV instruments, and pointed, target of opportunity (ToO) instruments. For a wide-FoV detector, the temporal and sky-coverage are large enough that the desired detection rate is achieved through low sensitivity and long-duration observations. This search discovers SNe independent of optical SN searches and is capable of detecting any escaping emission from the moment of explosion. This approach was employed by the SMM/GRS which detected 847/1238 keV emission from SN 1987A (Matz et al. 1988).³ Narrow FoV detectors rely upon triggers (optical detections) to observe ToO SNe. These

³The diagnostic utility of prompt emission was exemplified by the SMM/GRS studies of SN 1987A. The line appeared earlier than expected which suggested that ^{56}Ni may have been mixed outward in the ejecta. The total ^{56}Ni agreed with values suggested by light-curve studies.

instruments are engineered to have maximal sensitivity as a trade-off for the narrower FoV. The critical element in this approach is the time delay between the optical SN detection (and SN type identification) and the re-orientation of the gamma-ray instrument to observe the SN.

As is evident in Figure 1, the dominant prompt emissions are the $^{56}\text{Ni} \rightarrow ^{56}\text{Co}$ decays and the subsequent $^{56}\text{Co} \rightarrow ^{56}\text{Fe}$ decays. Type II SNe produce less ^{56}Ni than type Ia SNe (compare the peaks of the 812 & 847 keV lines in Figure 1) and have the ^{56}Ni buried under many solar masses of ejecta. For both of these reasons, prompt emission is far fainter in SNe II than SNe Ia. Figure 2 shows the time evolution of the line fluxes of the 812 & 847 keV lines for the same models shown in Figure 1. The SN Ia lines are much more intense than the SN II lines. Although the SN II rate is ~ 5 times larger than the SN Ia rate, the far larger flux for SNe Ia make them the dominant SN type for studies of *prompt* gamma-ray emission. For SNe Ia, the 812 keV line peaks sometime within the first 30 days after the explosion. ToO instruments would need to initiate observations no later than 13 days before the peak optical luminosity to fully study that feature. Current optical SN searches do not regularly detect SNe that early.⁴ SN searches would need to be dramatically improved to facilitate that requirement. A wide FoV instrument does not require an optical or any other external trigger.

The scientific insight that can be attained by studying the *prompt* emission from SNe Ia is the topic of this work, but longer-lived emissions are worthy of mention. The fluxes shown in Figure 2 suggest that *prompt* emission from SNe Ia can be detected to distances on the order of 100 Mpc by a detector capable of 10^{-7} photon $\text{cm}^{-2} \text{ s}^{-1}$ sensitivity. Barring a fortuitous galactic SN during the mission, prompt emission studies will investigate extra-galactic SNe.

Radionuclei with longer life-times emit at lower flux levels, but the emission from the nuclei may persist for centuries. The lower flux levels dictate that young SNRs can only be detected out to the Local Group. Older SNRs must be galactic, but the emission can be detected on decadal- millennial time-scales. *SNR* studies thus concentrate upon ^{57}Co (122 keV), ^{22}Na (1275 keV), ^{60}Co (1173,1332 keV), and ^{44}Ti (68,78,1157 keV). The ^{57}Co (122 keV) line was detected from SN 1987A, a young SNR in the LMC by the CGRO/OSSE instrument (Kurfess et al. 1992). The ^{44}Ti (1157 keV) line was detected from the galactic SNRs, Cas A (Iyudin et al. 1994) and RX J0852-4642 (Iyudin et al. 1998), by the CGRO/COMPTEL instrument.⁵ The SN 1987A detection suggests that the ^{57}Co decay rate was too low to explain the 1600 day optical luminosity. The Cas A detection suggests more ^{44}Ti production than was expected from the apparently low-luminosity SN observed by Flamsteed. The RX J0852-4642 detection motivated an archival search of ROSAT x-ray data to discover a “new” young SNR (Aschenbach et al. 1998). A next-generation gamma-ray telescope will contribute to the study of SNRs by detecting gamma-ray emission from many more SNRs (both historical and undiscovered) and by improving the flux estimates of previously detected SNRs. In addition, the improved angular resolution will allow studies of the spatial extent of the emission for bright, distributed SNRs.

Very long-lived radioactivities decay at relatively low rates. For the nearest SNRs, ^{26}Al and ^{60}Fe

⁴The difficulties of relying upon optical triggers was demonstrated by the CGRO/COMPTEL & OSSE observations of SN 1998bu. The SN was discovered nine days before peak, but CGRO observations began eight days later. The SN was observed for 88^d, but was not detected in gamma-ray line emission (Georgii et al. 1999).

⁵Recent analyses have lowered the significance of the 1157 keV line detection from RX J0852-4642 to the 2σ - 4σ level (Schönfelder 1999).

may be detectable similar to the ^{57}Co , ^{22}Na , ^{60}Co and ^{44}Ti emission. For these SNRs the 1809/1173 ratio is a discriminant between SN types. The 10^6 year life-times of these radionuclei dictate that the majority of detectable SNe will be too old to be resolved as individual SNRs. The study of this *diffuse* emission will investigate the cumulative contributions of 10,000 or more SNe. Maps of this emission are then the integrated million-year history of all SNe in the Galaxy (Diehl et al. 1995, Oberlack et al. 1996, Knodlseder et al. 1999). The 511 keV line emission from the annihilation of positrons produced in the decays of ^{56}Co , ^{44}Ti and ^{26}Al will also produce a diffuse emission (see Chan and Lingenfelter 1993 for a review of potential positron sources). Studies of diffuse emission contribute important information for models of galactic chemical evolution.

2 Estimate Parameters

2.1 Specifications of an ACT

NASA's Gamma-Ray Working Group (GRAPWG) has identified (June 1999) the study of nuclear astrophysics and sites of gamma-ray line emission as its highest priority science topic, and the development of an Advanced Compton Telescope (ACT) as its highest priority major mission. This instrument will follow three other instruments optimized to perform gamma-ray SN studies. The first generation Compton telescope was the COMPTEL instrument, which operated on-board the Compton Gamma-Ray Observatory (CGRO) from 1991-2000. COMPTEL used a liquid scintillator to produce a single Compton scatter and a NaI scintillator to capture the scattered energy. That combination achieved an instrumental angular resolution on the order of 2-4 degrees rms, and an energy resolution of 5-8 % FWHM. COMPTEL had a FoV of almost 60° , and observed SNe as targets of opportunity (ToO). COMPTEL may have marginally detected the 847 keV and 1238 keV ^{56}Co lines from the SN 1991T (Morris et al. 1997). The OSSE instrument, also on-board CGRO, used four NaI(Tl)-CsI(Na) scintillators to observe SNe as a ToO detector. OSSE had a 9% energy resolution and used a tungsten collimator to achieve a $3.8^\circ \times 11.4^\circ$ FWHM FoV. OSSE observations of SN 1991T and 1998bu did not detect either of the ^{56}Co decay lines. The SPI instrument on-board the INTEGRAL satellite will employ a coded-aperture germanium detector to observe gamma-rays in the 20 keV -2 MeV energy range. SPI is expected to achieve an angular resolution of 2-3 degrees FWHM, and an energy resolution of 2 keV (@ 1 MeV). The SPI instrument will have a narrow FoV (16°), that will be used as a ToO instrument for prompt SN science. The IBIS instrument, also on-board the INTEGRAL satellite, will also be capable of detecting broad-line gamma-ray emission with sensitivities almost equivalent to SPI.

The GRAPWG has outlined a baseline ACT with a goal of achieving a point source localization accuracy of $\sim 0.1^\circ$, an energy resolution of ≤ 3 keV (@2 MeV), a FoV of 60° and a broad-line sensitivity of 1×10^{-6} phot $\text{cm}^{-2} \text{s}^{-1}$ (10^6s , 3σ). The Naval Research Laboratory (NRL) is investigating both germanium and silicon Compton telescope designs, with the intention of exceeding the baseline specifications in both sensitivity and FoV (Kurfess et al. 1999). The advances that will make this improvement possible are: 1) large volume detector arrays which will increase the effective area, 2) excellent spatial and energy resolution from the use of position-sensitive solid-state detectors, and 3) employing two Compton scatters and a third interaction to determine the incoming energy and angle rather than a single scatter and total energy absorption (as employed with COMPTEL).

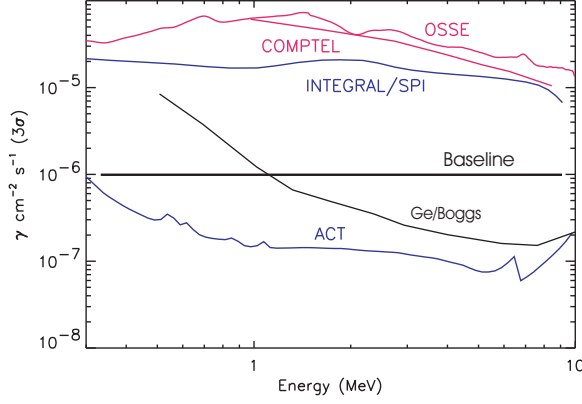


Figure 3. The sensitivity curves of the ACT and four other gamma-ray detectors. The curves are 3σ for 10^6 second accumulation.

The current NRL/ACT design will increase the FoV to 120° , and improve the broad-line sensitivity to 3×10^{-7} phot $\text{cm}^{-2} \text{s}^{-1}$ (10^6s , 3σ). The point source localization will be poorer than the baseline, increasing to 0.5 degrees for the weakest sources, but improves for strong sources. The energy resolution is expected to be ~ 20 keV. Boggs & Jean (2000) performed a simulation to estimate the sensitivity of a germanium Compton telescope. The telescope sensitivity was based on a background estimate for high-Earth orbit, and the efficiency derived from a simulation. Good events are those that undergo 3 or more interactions and are totally absorbed. Shown in Figure 3 are the broad-line sensitivity curves for the instruments described above.⁶ The sensitivity degrades significantly below 500 keV, making the 478 and 511 keV lines the lowest energy lines anticipated to be detectable.

If the ACT is placed in an equatorial, low-Earth orbit and scans along the celestial equator, as shown in Figure 4, it will observe roughly 87% of the sky every orbit, with a source within the FoV 1/3 of the time. By contrast, a 60° FoV instrument in the same orbit would observe 51% of the sky with one-sixth accumulation efficiency. Included in the FoV will be the Virgo Cluster (a likely region for SNe detections) and the Galactic Center (for studies of galactic gamma-ray sources). This strategy has two advantages. For prompt emissions, the telescope will be able to observe the SN *before* optical discovery, thus collecting photons on the rising and fading sides of the peaks. For SNR emissions, the telescope will revisit the remnant every orbit over the entire mission. This will lead to a composite observation with exposure far in excess of the 10^6s typical for a ToO observation.

Ideally, a wide-FoV optical instrument would accompany the Compton telescope, observing the same fields. The optical monitor would insure that all SNe would be observed every orbit from the time of explosion. Larger, ground-based telescopes would respond to gamma and optical triggers, providing follow-up spectra, light curves and precise positions. This would insure that all SNe detected in gamma-rays would be well-studied in the standard wavelengths.

⁶The Boggs and Jean Ge simulation was scaled to low-Earth orbit assuming a lowering of the background by a factor of ten, and a 20 keV FWHM line width.

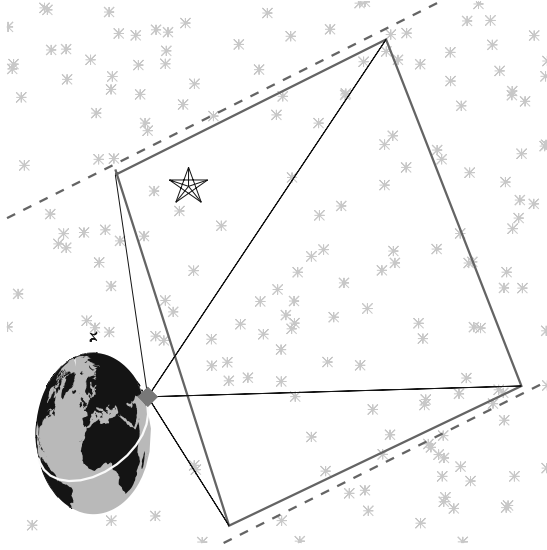


Figure 4. A schematic representation of the orbit of an ACT.

2.2 SN Ia Rate

SN rates are on the order of a few SNe per century per galaxy, meaning that many galaxies must be surveyed to produce a useable number of detections. SN searches have systematically observed galaxies and attempted to quantify the selection effects of their searches to derive the actual SN rate. SN rates are quoted in “SNU”, or the number of SNe per century per unit of blue luminosity ($10^{10} L_{\odot}^B$). SN rates depend upon the value of the Hubble constant, in this work we assume $H_0 = 68 \text{ km s}^{-1} \text{ Mpc}^{-1}$. Hamuy & Pinto (1999) estimated the rate to be $R = 0.23^{+0.33}_{-0.14} \text{ SNU } h_{68}^2$. Cappellaro et al. (1997) estimated the rate to be $R = 0.18 \pm 0.06 \text{ SNU } h_{68}^2$. Hardin et al. (2000) estimated the rate to be $R = 0.20^{+0.16}_{-0.09} \text{ SNU } h_{68}^2$. Averaging these estimates, we assume the rate to be $R = 0.2 \text{ SNU}$. To convert this value to a rate per volume, the luminosity density must be known. Hamuy & Pinto (1999) quoted Marzke, claiming the luminosity density to be $L_B = (1.12 \pm 0.29) \times 10^{-2} h_{68} (10^{10} L_{\odot}^B \text{ Mpc}^{-1})$.⁷ Combining these estimates suggests there are *100 SNe Ia per year within 100 Mpc*.

The 812 & 847 keV line fluxes shown in the next section suggest that SNe Ia will be detectable out to 100 -200 Mpc. The previous studies cited all sampled galaxies within roughly the same volume.⁸ We will assume that the SNe Ia density is uniform throughout the entire volume for the following estimates.

SNe Ia are not a homogeneous class. Individual SNe have been both brighter and fainter than

⁷Lin et al. 1996 claim a lower value, $L_B = (0.95 \pm 0.10) \times 10^{-2} h_{68} (10^{10} L_{\odot}^B \text{ Mpc}^{-1})$.

⁸The Cappellaro et al. (1997) search had a mean recession velocity of $z \sim 0.01$ (64 Mpc). The Hardin et al. (2000) search was the deepest, and it operated out to $z \sim 0.1$ (440 Mpc).

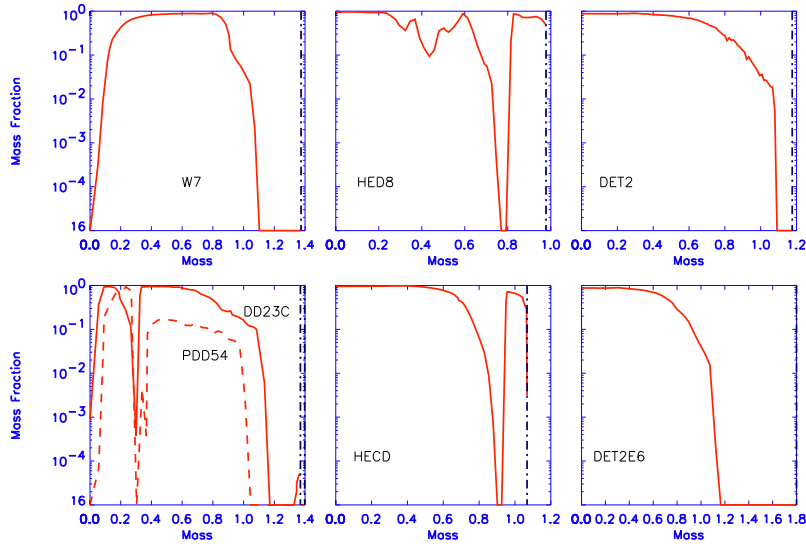


Figure 5. The radial distribution of ^{56}Ni for seven SN Ia models. The masses are in units of solar masses. The dashed lines denote the outer surface of the ejecta.

“normal” SNe. Li et al. (1999) suggests that only 60% of SNe Ia are normally-luminous (N), with 20% super-luminous (SP) and 20% sub-luminous (sb). We will use that 3:1:1 ratio in this work.

2.3 SN Ia Models

Considerable variations exist within the collection of SN Ia models. These variations are driven both by the uncertainty as to the correct explosion scenario(s) and by the heterogeneity displayed in the spectra and light curves of observed SNe Ia. While strong arguments have been made for and against each explosion scenario, the single-degenerate, Chandrasekhar mass scenario (SDCM) has emerged as the most plausible (Wheeler 1995, Livio 2000, Pinto & Eastman 2000b). We have included four SDCM models in our simulations; (1) the normally-luminous deflagration, W7, (2) the normally-luminous delayed detonation, DD23C (Höflich et al. 1998), (3) the sub-luminous pulsed-delayed detonation, PDD54 (Höflich, Khokhlov & Wheeler 1995), and (4) the super-luminous delayed detonation, W7DT (Yamaoka et al. 1992). The peak spectra of sub-Chandrasekhar mass models (SC) have been suggested to be too blue to explain SNe Ia (Nugent et al. 1995, Höflich & Khokhlov 1996), but the range of progenitor masses can naturally account for the peak-width/luminosity relation (Pinto & Eastman 2000a). We have included three variants of the SC scenario; (1) the normally-luminous SC model, HED8 (0.96 M_{ej} , 0.51 $M(^{56}\text{Ni})$), (2) the sub-luminous SC model, HED6 (0.77 M_{ej} , 0.26 $M(^{56}\text{Ni})$, Höflich & Khokhlov 1996), (3) the super-luminous SC model, HECD (1.07 M_{ej} , 0.72 $M(^{56}\text{Ni})$ Kumagai & Nomoto 1997). A double degenerate scenario involving the merger of two CO white dwarfs has also been suggested to explain SNe Ia. Disagreements as to

whether this “double degenerate” (DD) scenario leads to a SN Ia or an accretion-induced collapse (AIC) are on-going. An equally serious objection has been the failure to detect enough progenitor systems, although recent studies hint that enough DD SNe Ia could occur. We have included three variants of the DD scenario; DET2, DET2ENV2, and DET2ENV6.⁹ The ^{56}Ni distributions for 7 of the 10 models are shown in Figure 5. The DD models bury the ^{56}Ni under 0.6 -1.2 M. of ejecta, whereas SC models feature large amounts of ^{56}Ni near the surface. A small variation is shown within the SDCM group, where DD23C (and W7DT) have ^{56}Ni nearer the surface than does W7.

The gamma-ray line photons from the ^{56}Ni & ^{56}Co decays are either Compton scattered to lower energy or escape the ejecta. We simulate the scattering adopting the prescription of Podznyakov, Sobol & Sunyaev (1983). A detailed description of the Monte Carlo algorithm and its application in calculating the spectra and bolometric light curves of SN 1987A and Type Ia SNe have been presented by The, Burrows & Bussard (1990) and Burrows & The (1990). Shown in Figure 6 are the 812 & 847 keV line fluxes for the ten models, as would be observed from 10 Mpc. The 812 keV line peaks early and is a probe of the mass overlying the outermost ^{56}Ni -rich ejecta. The 847 keV line peaks later (at which time the ejecta for most models has become optically thin) and probes the total ^{56}Ni production. The solid lines are line fluxes calculated in this work, dashed lines and dot-dashed lines are results from other investigators. It is clear that our results, as well as Pinto & Eastman’s results, predict lower fluxes than either Höflich, Khokhlov & Wheeler (1998) (hereafter HKW), or Kumagai & Nomoto (1997). Our 847 keV line fluxes converge to the HKW fluxes at late times. Additionally, the energy deposition rates of HKW match well our calculations. Current efforts are being made to understand and resolve the discrepancies. Note that our results suggest fewer SN detections than the HKW and Kumagai results would suggest.

Concentrating upon our results, there are clear differences between the explosion scenarios. The flux ratio of the 812 keV line peak to the 847 keV line peak is a distance-independent discriminant. DD models feature very low 812/847 ratios, SC models feature high ratios. When combined with estimates of the host galaxy’s distance, the 847 keV peak flux can determine the ^{56}Ni production and thus discriminate between SDCM & SC scenarios. In the next section, we quantify these tendencies to suggest the rate at which different levels of science can be achieved with an ACT.

3 SN Ia Science with an ACT

An ACT will be capable of performing various degrees of scientific investigation of prompt emission from SNe Ia, depending upon the SN distance. For this work, we categorize the science as *detections*, *discrimination*, and *diagnostics*, and describe each category separately.

3.1 Detections

Gamma-ray detection of SNe Ia will be the most basic level of science that will be performed with an ACT. Through SN detections we learn about the relative rates of SN Ia sub-classes (N,SP,sb), the SN Ia rate as a function of galaxy morphological class, and the projected radial distribution of SNe Ia. All of these studies assume that the gamma-ray observations are coordinated with optical

⁹Höflich et al. 1996 has shown that DD models do not follow the peak-width/luminosity relation.

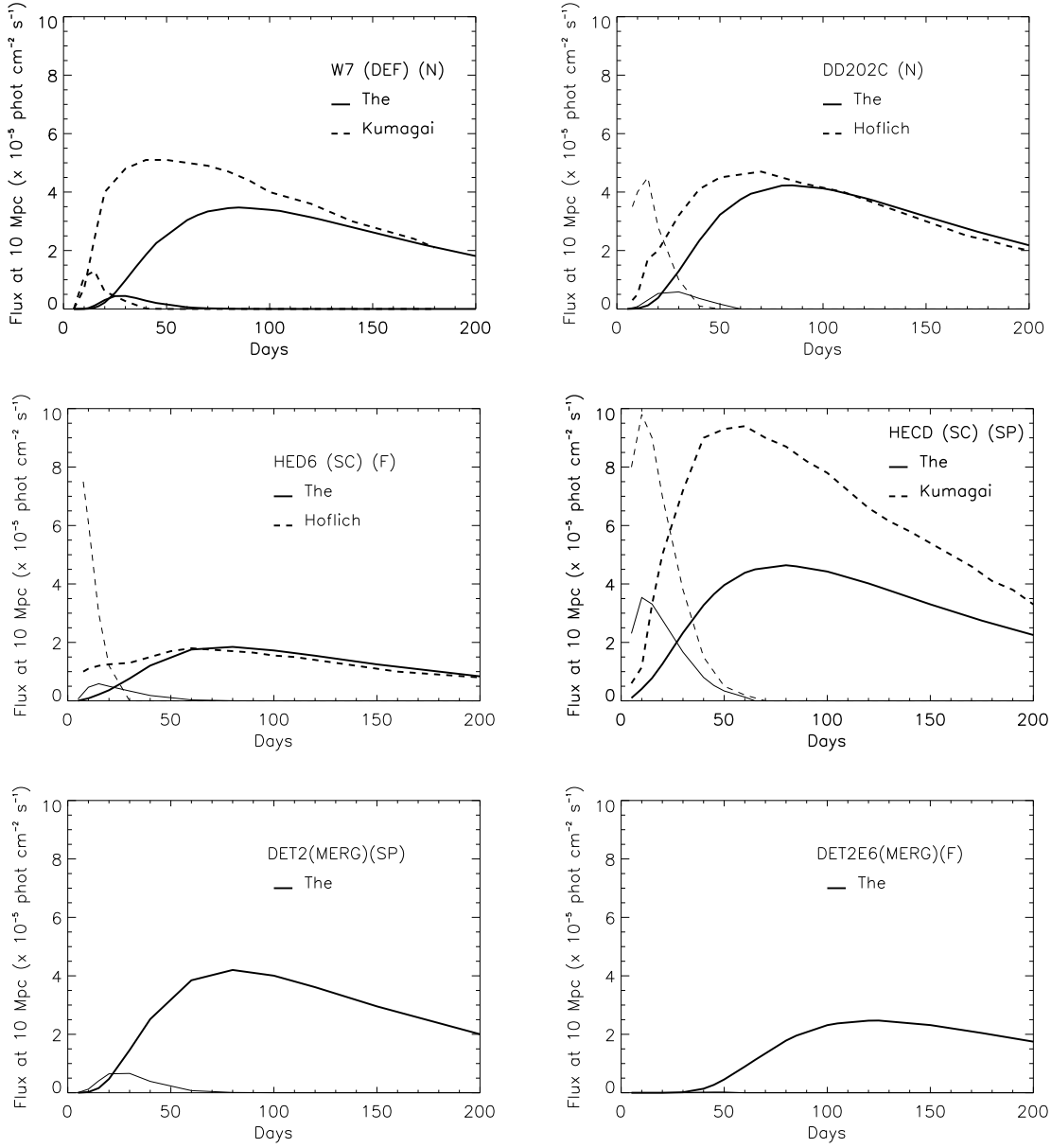


Figure 6. Gamma-ray lines fluxes for six SN Ia Models at 10 Mpc. The thin curves show 812 keV line fluxes, the thick lines show 847 keV line fluxes. The solid lines were calculated for this work, the dashed lines are from HKW or Kumagai & Nomoto 1997.

TABLE 1. Maximum detectable distance and detection rates for various SN Ia models.^{a,b}

Model	GRAPWG Baseline		NRL ACT Concept	
Name	Distance [Mpc]	Rate [SNe/yr]	Distance [Mpc]	Rate [SNe/yr]
Normal				
W7	57	5.8	123	97
HED8	60	6.5	128	110
DD23C	56	5.3	120	89
Sub-lum				
W7DT	69	3.4	148	57
HECD	67	3.1	145	53
DET2	62	2.5	134	42
Super-lum				
PDD54	30	0.3	65	4.8
HED6	41	0.7	89	12
DET2E6	50	1.1	103	19
Type II	750 kpc	—	1.6 Mpc	—

a Detections are at the 5σ level.

b Based on gamma-ray line fluxes shown in Figure 6.

observations. By detecting SNe both optically and in gamma-rays, we can get a measure of the selection biases of each SN search. Howell et al. (1999) demonstrates that optical SN searches (visual, photographic & CCD) suffer from the “Shaw effect”, where SNe in the inner bulges of galaxies are less frequently detected. Additionally, the optical emission from SNe suffers extinction from intervening dust. Highly extinguished SNe are less likely to be detected. Gamma-rays are not expected to suffer from these effects and will detect all SNe Ia in a galaxy. This information is particularly relevant to determining the SN contribution to galactic chemical evolution.

Many SNe need to be detected for the estimated SN rates and distributions to be significant. Shown in Table 1 are the distances and rates at which given SN models could be detected (5σ) via the combined observation of the 750, 812, 847, 1238 & 1562 keV lines. The estimates are made for both the GRAPWG baseline specifications and the enhanced sensitivity design being studied at NRL. For each ACT, the ^{56}Ni -rich super-luminous SNe Ia will be detected to the largest distances, but the larger SN rate of normally-luminous SNe Ia make them the most frequently sampled sub-class. The NRL-ACT will detect SNe Ia to roughly twice the distance as would the baseline ACT, and will detect ~ 160 SNe Ia/yr compared to ~ 10 SNe Ia/yr. We assert that a 5 year sampling of 800 SNe Ia will allow SN rate studies at a scientifically-interesting level, while 50 SNe Ia are inadequate.¹⁰

Detecting SNe with a wide FoV instrument depends upon the *integrated flux*. The differences between the simulations shown in Figure 6 occur principally at early times. Using the larger fluxes suggested by HKW and Kumagai would not lead to an appreciable increase in the number of detec-

¹⁰The NRL-ACT design detects more SNe than the baseline ACT due to a wider FoV and a better sensitivity.

TABLE 2. Rates at which pairs of SN Ia models would be distinguished.^a

GRAPWG Baseline			NRL ACT Concept		
	HED8	DD23C		HED8	DD23C
W7	0.9	0.1	W7	15	1.0
HED8	—	1.2	HED8	—	21
	HECD	DET2		HECD	DET2
W7DT	0.1	0.3	W7DT	1.7	5.8
HECD	—	0.5	HECD	—	8.3
	HED6	DET2E6		HED6	DET2E6
PDD54	0.1	0.0	PDD54	1.3	0.8
HED6	—	0.4	HED6	—	7.3

^a Rates are in units of [SNe/yr]. Detections are at the 3σ level.

tions.

3.2 Discrimination

For a subset of the detected SNe Ia, the line fluxes will be large enough to generate light curves. This will allow discrimination between the various models suggested to explain each sub-class. The estimated rate (per year) at which a given SN model could be distinguished from alternative models is shown in Table 2. This discrimination assumes that the explosion date is known to within ± 3 days from optical spectra obtained as part of a coordinated study. The NRL-ACT would be able to discriminate between SDCM models and SC models for 15-21 SNe Ia per year (or 75-100 over a 5 year mission lifetime). The deflagration (W7) could be distinguished from the delayed detonation (DD23C) once per year. Lower SN rates for SP and sb SNe Ia mean that SDCM and SC models will be distinguished 6-9 times for each sub-class by the better ACT (over a 5 year mission lifetime). By contrast, the baseline ACT will detect two SNe Ia per year with which it can distinguish between explosion scenarios. Again we assert that the increased sampling of the NRL-ACT relative to the baseline ACT will critically improve the useable science.

This information would conclusively establish which explosion scenario dominates SNe Ia. For normal SNe Ia, if none of the 100 or so of these nearby SNe were best explained by an alternative scenario, than that scenario could be effectively rejected. Note that discrimination between SN explosion scenarios is critically dependent upon the gamma-ray transport simulations. It is for this application of an ACT that simulation discrepancies must be resolved.

3.3 Diagnostics

For very nearby SNe Ia, the evolution of the ejecta may be studied in greater detail. Chan & Lingenfelter (1988), Bussard, Burrows, & The (1989), Burrows & The (1990), and HKW demonstrated

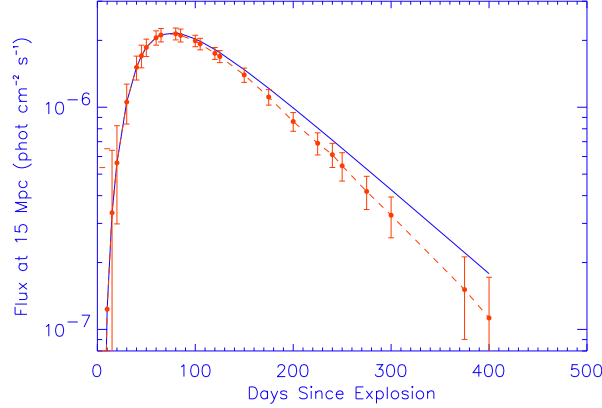


Figure 7 The 511 keV line flux for a SN Ia at 15 Mpc assuming two positron transport scenarios. The dashed line, with simulated observations, was calculated assuming positron escape. The solid line, which would scale with the 847 keV line, assumes instantaneous, in-situ positron annihilation.

that both the line centroid, the line width, and the line profile of gamma-ray lines probe the kinematics of the ejecta and reveal the velocity distribution of the ^{56}Ni in the ejecta. Qualitatively, the line centroid will be initially blue-shifted due to detection of only the gamma-ray photons from the approaching face on the SN. As the ejecta thins to gamma-rays, the line centroid moves to the energy dictated by the host galaxy’s red-shift. Most SN Ia models have the ^{56}Ni -rich ejecta in the inner regions. For these SN models, the thinning of the ejecta with time reveals an increasing range of velocities. This produces a widening of the gamma-ray lines with time, with the FWHM asymptotically approaching the FWHM dictated by the mean ^{56}Ni velocity. The only exceptions to this are the SC models dominated by ^{56}Ni near the surface (HED6). Those SN models feature an initially broad line that subsequently narrows and then slowly broadens to the FWHM dictated by the mean ^{56}Ni velocity. Characterizing the line profile/shape in general, for a radioactive source distributed in a thin shell, the gamma line profile at maximum has a box shape, while a uniformly distributed source has a parabolic shape (Burrows & The 1990). Quantitatively, the blue-shift decreases from ~ 20 keV to 0 keV, and the line width increases from ~ 15 keV to ~ 30 keV.

Whereas these effects will need to be included in the analysis to properly estimate line fluxes, it is uncertain whether the ACT designs under development will be able to discriminate between SN models based upon these features. The differences between the centroids are typically less than 4 keV, the FWHM of the models vary by typically 8 keV (the largest variation is between HED6 and PDD5, which differ by 20 keV FWHM at 8^d). Optimizing the ACT in light of these effects will be one of the challenges facing ACT designers, requiring a combination of high sensitivity and good energy resolution.

Hard X-ray spectra and the K X-ray line fluxes can be used to infer the composition or metallicity of the ejecta (The, Clayton, & Burrows 1990; The, Bridgman, & Clayton 1994). X-ray band flux

ratios reflect the slope of the X-ray spectrum and the scattering and photoelectric opacities of the ejecta. The time evolution of the X-ray band flux ratios and the ratios of the total X-ray and gamma-line luminosities can also reveal the extent of mixing or clumping in the ejecta.

An additional diagnostic that can be studied with an ACT is the magnetic field of the ejecta. The decay of $^{56}\text{Co} \rightarrow ^{56}\text{Fe}$ which produces the 847 & 1238 keV lines also produces positrons in 19% of the decays. Initially, the positrons have negligible lifetimes, producing two 511 keV annihilation photons that will scale with the 847 keV line. By 100^d , if the magnetic field is either too weak to confine positrons, or radially-combed permitting positrons to escape along the field lines, then the 511/847 line ratio will decrease as positrons escape the ejecta. If the field is strong and turbulent, the 511/847 ratio will remain constant. Milne, The & Leising (1999), Capellaro et al. 1997, and Ruiz-Lapuente & Spruit (1998) have all transported positrons through SN Ia models and compared model-generated optical light curves to observations of type Ia SNe. All three groups conclude that positrons may escape the ejecta, although disagreement exists whether this is a general result for every SN Ia. Figure 7 shows the 511 keV line flux for the SN Ia model, HED8 at 15 Mpc. The dashed line, with simulated data, shows the line flux if the magnetic field is such that positrons are allowed to escape. The solid line shows the line flux if positrons are trapped and annihilate in-situ (which would follow the 847 keV line). Assuming that the ACT sensitivity is $6 \times 10^{-7} \text{ phot cm}^{-2} \text{ s}^{-1}$ ($3\sigma, 10^6\text{s}$) to 511 keV broad-line emission, this could be detectable above the 4σ level to 15 Mpc for the SC model, HED8, to 10 Mpc for the SDCM model, DD23C. If a very nearby SN Ia occurs, the direct determination of positron escape/trapping may be made.

4 Conclusions

The ejecta of SNe Ia is profoundly radioactive. Measuring the gamma ray emission from SN ejecta is a useful probe of the nucleosynthesis and hydrodynamics (energetic, structure, mixing/clumping) of the SN explosion, and thus is a discriminant between explosion scenarios. Although gamma-ray line emission is observable for more than a millennium from nearby SNRs, in this work we concentrate upon the science that can be realized from the study of prompt decays. The decays of $^{56}\text{Ni} \rightarrow ^{56}\text{Co} \rightarrow ^{56}\text{Fe}$ produce a number of prompt gamma-ray lines which an ACT could detect to distances greater than 100 Mpc. The wide FoV of the ACT design is particularly suitable for the study of SNe Ia. We show that the current estimates of the SN Ia rate suggests that many SNe will be detected by such an instrument. We argue for the production of an ACT capable of wider FoV observations and improved sensitivity than the baseline design suggested by the GRAPWG. We feel that the rates of detection and discrimination achievable with the NRL ACT concept are large enough to make that instrument a landmark astrophysical tool.

The time-frame of the development of an ACT is on the order of a decade. During that time, the field of SN Ia science will certainly advance. In particular, the efficiency of SN searches will appreciably improve. The design of the ACT must exploit the anticipated advances to best utilize the gamma-ray information that will be accumulated. Advances in optical studies will not remove the necessity of gamma-ray line observations. It is closer to the truth to assert that the combined constraints from optical and gamma-ray investigations will exceed the sum of the individual constraints. The potential of this instrument are exciting to contemplate.

REFERENCES

- Aschenbach, B. 1998, *Nature*, 396, 141
- Bodansky, D., Clayton, D.D., Fowler, W.A. 1968, *ApJS*, 16, 299
- Boggs, S.E., Jean, P.J., in *Proceedings of the 4th INTEGRAL Workshop*, in press
- Burrows, A. and The, L.-S. 1990, *ApJ*, 360, 626
- Capellaro, E. et al. 1997, *A&A*, 322, 431
- Chan, K.-W., Lingenfelter, R.E. 1993, *ApJ*, 405, 614
- Colgate, S.A., White, R.H. 1966, *ApJ*, 143, 626
- Diehl, R. et al. 1995, *A&A*, 298, 445
- Georgii, R. et al. 1999, in *Proceedings of the 5th Compton Symposium*, ed. M.L. McConnell & J.M. Ryan, (New York:AIP), p.49
- Hamuy, M., Pinto, P.A. 1999, *AJ*, 117, 1185
- Hardin, D. et al. 2000, *A&A*,
- Höflich, P., Khokhlov, A., Wheeler, J.C. 1995, *ApJ*, 444, 831
- Höflich, P., Khokhlov, A. 1996, *ApJ*, 457, 500
- Höflich, P., Wheeler, J.C., Theilemann, F.-K. 1998, *ApJ*, 495, 617
- Howell, A., Wang, L., Wheeler, J.C. 1999, *astro-ph*, 9908127
- Iyudin, A.F. et al. 1994, *A&A*, 284, L1
- Iyudin, A.F. et al. 1998, *Nature*, 396, 142
- Knodlseder, J. et al. 1999, *A&A*, 345, 813
- Kumagai, S., Nomoto, K. 1997, in *Proceedings of the NATO ASI on Thermonuclear Supernovae (C486)*, ed. P. Ruiz-lapuente, R. Canal, J. Isern, (Dordrecht: Kluwer), p. 515
- Kurfess, J.D. et al. 1992, *ApJ*, 399, L137
- Li, W.D. et al. 1999, in *Proceedings of the 10th Maryland Astrophysics Conference*, ed. S.S. Holt & W.H.Zhang, (New York:AIP), p.91
- Lin, H. et al. 1996, *ApJ*, 464, 60
- Livio, M. 2000, *astro-ph*, 0005344, 22 pages
- Marzke, R.O., et al. 1998, *ApJ*, 503, 617
- Matz, S.M. et al. 1988, *Nature*, 331, 416
- Milne, P. A., The, L.-S., and Leising, M. D. 1999, *ApJS*, 124, 503
- Morris, D.J. et al. 1997, in *Proceedings of the 4th Compton Symposium*, ed. C.D. Dermer, M.S. Strickman, J.D. Kurfess, (New York:AIP), p.1084
- Nomoto, Thielemann, F.-K., Yokoi, K. 1984, *ApJ*, 286, 644
- Nugent, P. et al. 1995, *ApJ*, 441, L33
- Oberlack, U. et al. 1996, *A&AS*, 120C, 311
- Pinto, P.A., Woosley, S.E. 1988, *ApJ*, 329, 820
- Pinto, P.A., Eastman, R.G. 2000a, *ApJ*, 530, 744
- Pinto, P.A., Eastman, R.G. 2000b
- Pinto, P.A., Eastman, R.G., Rogers, T. 2000,
- Pozdnyakov, L. A., Sobol, I. M., and Sunyaev, R. A. 1983, *Ap. Space. Phys. Rev.*, 2, 189
- Ruiz-Lapuente, P., and Spruit, H. 1998, *ApJ*, 500, 360
- Schönfelder, V. et al. 1999, in *Proceedings of the 5th Compton Symposium*, ed. M.L. McConnell & J.M. Ryan, (New York:AIP), p.54

- The, L.-S., Bridgman, W. T., and Clayton, D. D. 1994, *ApJS*, 93, 531
- The, L.-S., Burrows, A., and Bussard, R. W. 1990, *ApJ*, 352, 731
- The, L.-S., Clayton, D. D., and Burrows, A. 1990, in *IAU Symp. 143, Wolf-Rayet Stars in Galaxies*, ed., K. A. van der Hucht & B. Hidayat (Dordrecht: Kluwer), 537
- Truran, J.W., Arnett, W.D., Cameron, A.G.W. 1967, *Can. J. Phys.*, 45, 2315
- Wheeler, J.C. 1995, in *Proceedings of the NATO ASI on Evolutionary Processes in Binary Stars (C477)*, ed. R.A.M.J. Wijers, M.B. Davies, C.A. Tout, (Dordrecht: Kluwer), p. 307
- Woosley, S. E., Pinto, P. A., and Hartmann, D. H. 1989, *ApJ*, 346, 395
- Yamaoka, H., et al. 1992, *ApJ*, 393, L55